ADVANCED MATERIALS
www.advmat.de

Hydration-Effect-Promoting Ni–Fe Oxyhydroxide Catalysts for Neutral Water Oxidation

Ning Wang, Zhen Cao, Xueli Zheng, Bo Zhang, Sergey M. Kozlov, Peining Chen, Chengqin Zou, Xiangbin Kong, Yunzhou Wen, Min Liu, Yansong Zhou, Cao Thang Dinh, Lirong Zheng, Huisheng Peng, Ying Zhao, Luigi Cavallo, Xiaodan Zhang,* and Edward H. Sargent**

Oxygen evolution reaction (OER) catalysts that function efficiently in pH-neutral electrolyte are of interest for biohybrid fuel and chemical production. The low concentration of reactant in neutral electrolyte mandates that OER catalysts provide both the water adsorption and dissociation steps. Here it is shown, using density functional theory simulations, that the addition of hydrated metal cations into a Ni–Fe framework contributes water adsorption functionality proximate to the active sites. Hydration-effect-promoting (HEP) metal cations such as Mg^{2+} and hydration-effect-limiting Ba^{2+} into Ni–Fe frameworks using a room-temperature sol–gel process are incorporated. The Ni–Fe–Mg catalysts exhibit an overpotential of 310 mV at 10 mA cm^{-2} in pH-neutral electrolytes and thus outperform iridium oxide (IrO_2) electrocatalyst by a margin of 40 mV. The catalysts are stable over 900 h of continuous operation. Experimental studies and computational simulations reveal that HEP catalysts favor the molecular adsorption of water and its dissociation in pH-neutral electrolyte, indicating a strategy to enhance OER catalytic activity.

Water oxidation is of prime importance in electrochemical water splitting and CO_2 reduction technologies.[1] Thanks to an intensive worldwide effort, its performance has advanced continuously in recent years.[2–4] Since a pH-neutral environment is required for biological growth, water oxidation should function efficiently in neutral pH if it is to enable ever-higher-performing biohybrid systems for the synthesis of fuels and chemicals using renewable energy.[5,6]

Unfortunately, the overpotential for the oxygen evolution reaction (OER) is in general very high (>460 mV at 10 mA cm^{-2})[7–10] under neutral pH. As a result, bioelectrolysis systems have exhibited low power conversion efficiencies. The neutral OER problem is particularly challenging since, in pH-neutral electrolytes, the reactant concentration

Dr. N. Wang, Dr. X. Kong, Prof. Y. Zhao, Prof. X. Zhang
Institute of Photoelectronic Thin Film Devices and Technology of Nankai University
Tianjin 300350, P. R. China
E-mail: xdzhang@nankai.edu.cn

Dr. N. Wang, Dr. X. Kong, Prof. Y. Zhao, Prof. X. Zhang
Key Laboratory of Photoelectronic Thin Film Devices and Technology of Tianjin
Tianjin 300350, P. R. China

Dr. N. Wang, Dr. X. Kong, Prof. Y. Zhao, Prof. X. Zhang
Collaborative Innovation Center of Chemical Science and Engineering
Tianjin 300350, P. R. China

Dr. N. Wang, Dr. X. Kong, Prof. Y. Zhao, Prof. X. Zhang
Renewable Energy Conversion and Storage Center of Nankai University
Tianjin 300072, P. R. China

Dr. N. Wang, Dr. X. Zheng, Dr. P. Chen, Dr. C. Zou, M. Liu, Dr. Y. Zhou, Dr. C. T. Dinh, Prof. E. H. Sargent
Department of Electrical and Computer Engineering
University of Toronto
35 St George Street, Toronto, Ontario M5S 1A4, Canada
E-mail: ted.sargent@utoronto.ca

The ORCID identification number(s) for the author(s) of this article can be found under https://doi.org/10.1002/adma.201906806.

DOI: 10.1002/adma.201906806

Dr. Z. Cao, Prof. S. M. Kozlov, Prof. L. Cavallo
Physical Sciences and Engineering Division (PSE)
KAUST Catalysis Center (KCC)
King Abdullah University of Science and Technology (KAUST)
Thuwal 23955-6900, Saudi Arabia

Prof. B. Zhang, Prof. P. Chen, Dr. Y. Wen, Prof. H. Peng
State Key Laboratory of Molecular Engineering of Polymers
Department of Macromolecular Science and Laboratory of Advanced Materials
Fudan University
Shanghai 200438, China
E-mail: bozhang@fudan.edu.cn

Prof. L. Zheng
Beijing Synchrotron Radiation Facility
Institute of High Energy Physics
Chinese Academy of Sciences
Beijing 100049, China

is several orders of magnitude lower than in the alkaline electrolyte.[11] OER in pH-neutral electrolyte therefore requires additional water adsorption and dissociation processes to provide the adsorbed water molecules (H_2O^*)—and the OER steps under neutral-pH conditions[12]

$$H_2O^* \rightarrow OH^* + H^+ + e^- \quad (1)$$

$$OH^* \rightarrow O^* + H^+ + e^- \quad (2)$$

$$O^* + H_2O^* \rightarrow OOH^* + H^+ + e^- \quad (3)$$

$$OOH^* \rightarrow * + O_2 + H^+ + e^- \quad (4)$$

Catalysts including iridium oxide (IrO_2)[13] as well as Co-based,[14] Ni-based,[15,16] and Mn-based[17] materials, have each shown recent progress in OER performance in pH-neutral electrolytes. Nevertheless, these catalysts have yet to fulfill the requirement of sub-350 mV overpotentials and prolonged durability (≥500 h typically for initial stability studies).[18]

We took the view that efficiently capturing and dissociating water molecules at the catalyst/water interface could improve OER performance in pH-neutral electrolytes. Prior studies have shown that noncovalent interactions between hydrated metal cations (M^{n+}) and *OH form OH_{ad}-$M^{n+}(H_2O)_x$ and enhance the adsorption of OH^- at the catalyst/electrolyte interface. These methods can accelerate the oxygen reduction reaction.[19–24] Mg^{2+} is an example of a metal that can support another beneficial strategy: it possesses a high hydration energy that offers the prospect of enhancing the bond strength between the catalyst surface and molecular water.[23] We hypothesized that introducing ions of this kind into the catalyst framework could lead to a higher hydration level of the system, improving thereby the OER rate.

Theoretical studies of the hydration effect on Ni–Fe based catalyst. Using the Ni–Fe system as a prototypical framework,[25,26] we investigated the effect of introducing metal cations with strong hydration capacity and small atomic diameters. We focus on whether water adsorption onto the surface of Ni–Fe catalyst can be enhanced.

We first studied the effect of Mg^{2+} (a relatively small size cation) and compared it with Ba^{2+} (a relatively large size cation) doping (**Figure 1**). In each case we examined the water adsorption properties of the doped Ni–Fe catalyst.

Starting from a stable metal oxyhydroxide model, we constructed the slab β-NiOOH as the catalyst framework (Figure S1, Supporting Information).[27,28] Mg atoms remain at the catalyst surface, and are directly exposed to the aqueous solution during OER (Figure S2, Supporting Information).

We then considered the immersion of this catalyst into aqueous solution: we assumed that two $(0\bar{1}5)$ facets were exposed to interfacial water. One of the two $(0\bar{1}5)$ facets was modified to replace half of the surface Ni^{2+} with the relatively small Mg^{2+} or the larger Ba^{2+} cations (Figure 1a,d), while the other facets of the catalyst were kept the same as controls. Water adsorption on each catalyst was investigated using molecular dynamic simulations in the canonical ensemble at 300 K (details in the Supporting Information). We accumulated a 12 ps trajectory and recorded the final 10 ps trajectory to produce a map of the water-catalyst distance under dynamic conditions. Specifically, we report $\left\langle \frac{1}{d\sqrt{\pi}} \exp\left(-\frac{(a_O - a_i)^2}{\xi^2}\right)\right\rangle$, where d is the shortest distance between the interfacial water oxygen and any metal ion at slab surface, a_O is the x–y coordinate of this water oxygen, a_i is the grid on the surface, and ξ = 1.0 Å determines the resolution of the map (Figure 1b,c,e,f).

In the absence of the Mg^{2+} cation, the surface OH terminal groups of the Ni–Fe catalyst determine the interfacial water

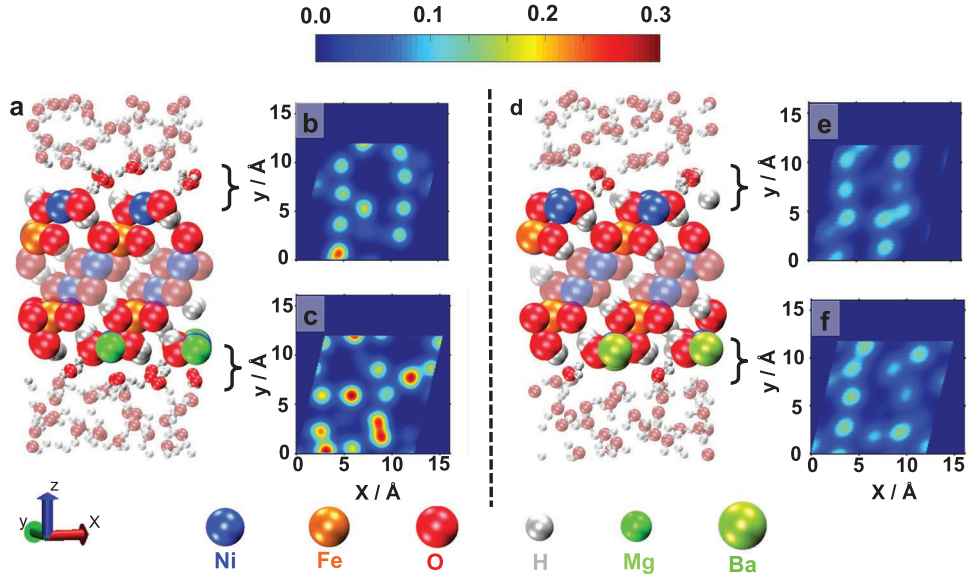

Figure 1. DFT simulation of hydration on simplified Ni–Fe framework surfaces with Mg^{2+} versus Ba^{2+} doping. a) Snapshot of Ni–Fe–Mg catalyst emerged in aqueous solution: the framework was constructed using the Ni–Fe–OOH catalyst, and four Mg^{2+} were inserted into one $(0\bar{1}5)$ facet. b,c) The closer water–oxygen–metal cation distance. d) Snapshot of Ni–Fe–Ba catalyst emerged in aqueous solution: the framework was constructed using the Ni–Fe–OOH catalyst, and four Ba^{2+} were inserted into one $(0\bar{1}5)$ facet. e,f) The water maps above the catalyst with or without surface Ba^{2+}.

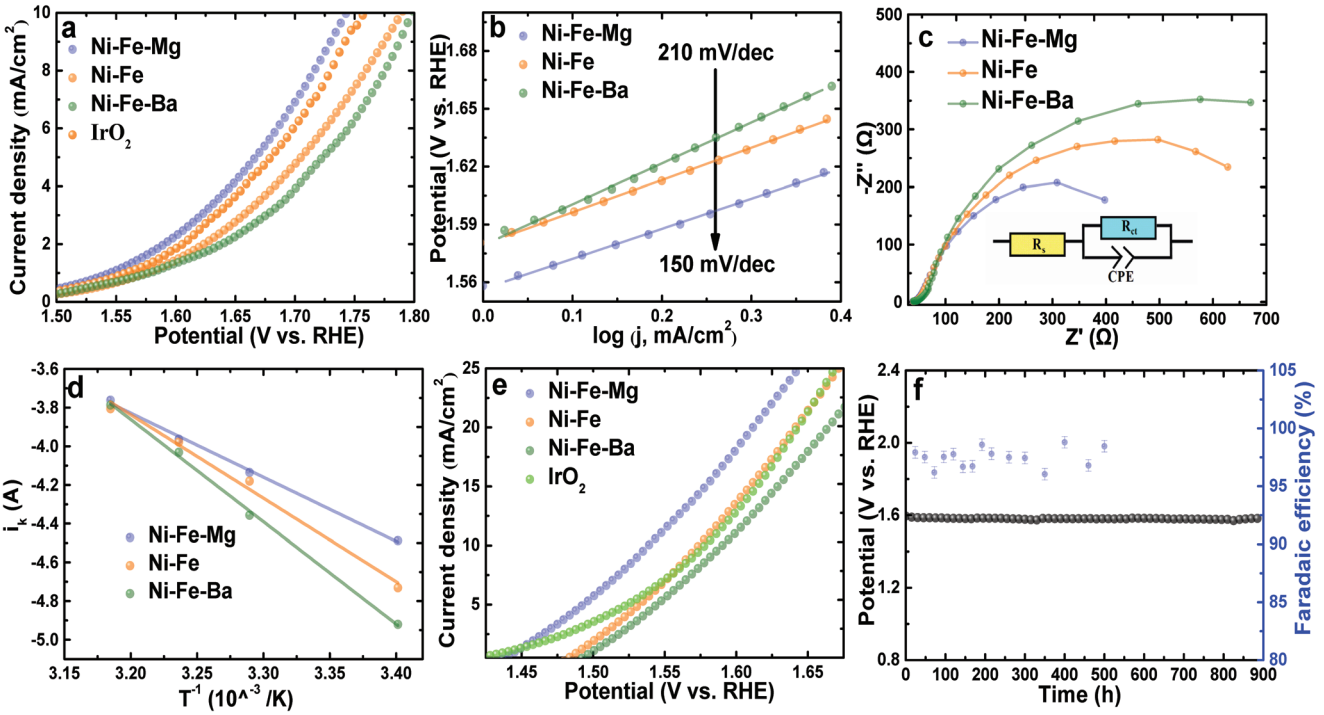

Figure 2. Performance of Ni–Fe–Mg catalyst and controls in a three-electrode configuration in CO_2 saturated 0.5 M $KHCO_3$ aqueous electrolyte. a) OER polarization curves for catalysts loaded on GCE. The data were obtained using 1 mV s^{-1} scan rate and are presented without *iR* correction (catalyst loading 0.21 mg cm^{-2}). b) Tafel plot of catalysts loaded on GCE. c) Electrochemical impedance spectroscopy (EIS) data for Ni–Fe–Mg catalysts and controls in three-electrode configuration in CO_2 saturated 0.5 M $KHCO_3$ aqueous electrolyte. The data were collected for the electrodes under 1.6 V versus RHE. The inset provides the equivalent circuit: R_s: series resistance; R_{ct}: charge-transfer resistance; CPE: constant-phase element related to the double-layer capacitance. d) Activation energy of samples on Ni foam obtained from the Arrhenius relationship. e) The OER polarization curves of Ni–Fe–Mg catalysts and controls loaded on Au-coated Ni foam in a three-electrode configuration in CO_2 saturated 0.5 M $KHCO_3$ aqueous electrolyte. f) Chronopotentiometric curves obtained from the Ni–Fe–Mg catalyst on Ni foam electrode with constant current densities of 10 mA cm^{-2}, and the corresponding Faradaic efficiency from gas chromatography measurement of evolved O_2.

distribution via hydrogen-bonding interactions. When surface Mg^{2+} is added, it attracts interfacial water molecules, leading to a shorter distance between the oxygen atom in water and the metal ions (red patches in Figure 1c). These interfacial water molecules no longer reflect the structure of surface OH terminal groups. By contrast, when Ba^{2+} is introduced, the water-catalyst distance is dominated by the hydrogen-bonding network (Figure 1f).

Using this simple model, we are able to suggest a trend: pursuing experimental doping using cations having a high hydration capacity could potentially offer more water molecules for dissociation reactions.

Synthesis and OER activity of hydration-effect catalysts. We synthesized hydration-effect-promoting (HEP) oxyhydroxides and hydration-effect-limiting (HEL) Ni–Fe–Ba oxyhydroxides. We used a room-temperature sol–gel process previously reported.[29] Energy-dispersive X-ray spectroscopy mapping shows a uniform distribution of Ni, Fe, and Mg (Figure S3, Supporting Information). From inductively coupled plasma optical emission spectra, we determined the molar ratio of Ni:Fe:Mg to be 7:1:0.2 (Figure S4, Supporting Information). The catalysts present a porous structure (Figure S5, Supporting Information) without evidence of crystallinity (Figure S6, Supporting Information).

We evaluated catalytic properties using a three-electrode electrochemical cell containing CO_2-saturated 0.5 M $KHCO_3$ electrolyte. Compared with the HEL catalyst, the HEP exhibited a significant improvement in catalytic activity on glass carbon electrode (GCE). Linear sweep voltammetry (LSV) polarization measurements indicate that optimized Ni–Fe–Mg requires only 514 mV overpotential to reach 10 mA cm^{-2} on GCE, which outperforms the best oxide catalysts previously reported (**Figure 2**a; Table S1 and Figure S7, Supporting Information). The decreased Tafel slope (210 mV dec^{-1}→150 mV dec^{-1}, Table S2, Supporting Information) indicates a higher OER reaction rate when Mg^{2+} is incorporated (Figure 2b). Charge-transfer resistance (R_{ct}), determined using electrochemical impedance spectroscopy (Figure 2c), shows that incorporating Mg^{2+} decreases the R_{ct} (580 → 480 Ω) and gives rise to faster electrode kinetics. The Ni is in an oxidation state higher than 3+ as seen in previous reports (Figure S8, Supporting Information).[30,31]

Next, we investigated further electrochemical behaviors of the best catalysts compared to controls in order to characterize intrinsic activity. First, we normalized the current density using the electrochemically active surface area (ECSA) obtained using the double-layer capacitance (C_{dl}) technique.[32,33] The ECSA-normalized current density of the HEP catalyst is fully 1.3-times and 1.8-times higher than those of reference Ni–Fe catalyst and HEL Ni–Fe–Ba catalyst, respectively, at 1.7 V versus RHE (Figure S9, Table S3, Supporting Information). The activation energy (Figure 2d) and turnover frequency[29,31,34–36]

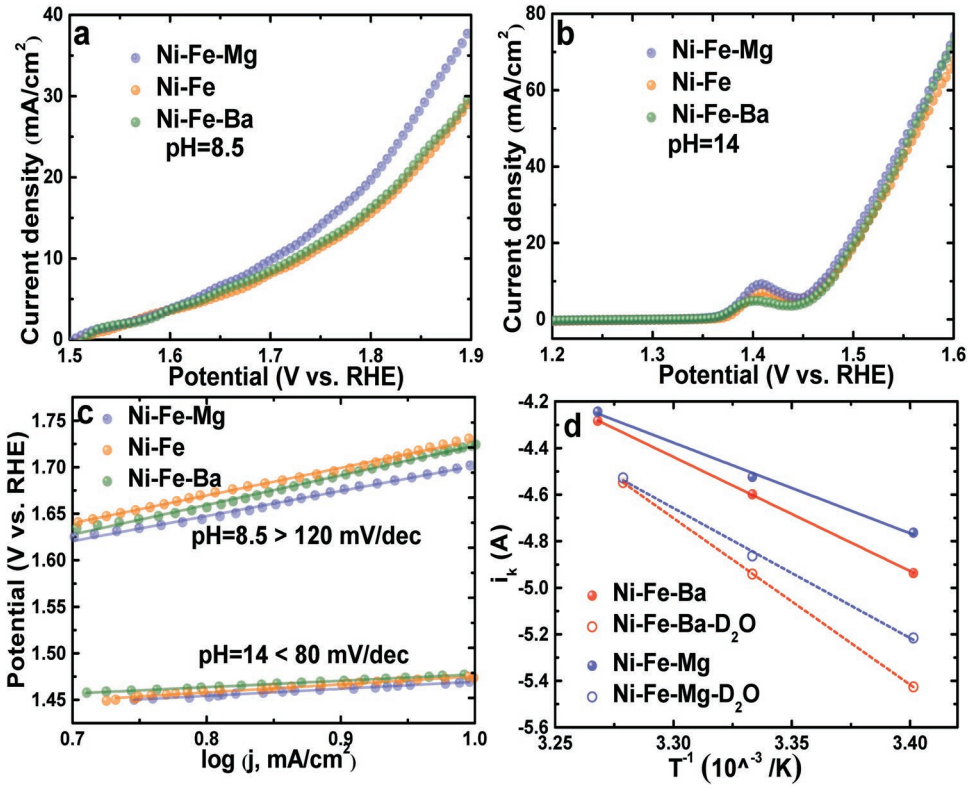

Figure 3. OER polarization curves of Ni–Fe–Mg catalyst and relevant controls. The materials were loaded on GCE in a) 0.5 M $KHCO_3$ (pH ≈ 8.5) and b) 1 M KOH electrolyte (pH ≈ 14). c) The corresponding Tafel curves of Ni–Fe–Mg catalyst in 0.5 M $KHCO_3$ (pH ≈ 8.5) and 0.5 M KOH electrolyte (pH ≈ 14). d) Arrhenius plot of the inverse temperature versus the log of the exchange current for Ni–Fe–Mg and Ni–Fe–Ba catalyst in electrolyte with H_2O and D_2O.

(TOF, Figure S10 and Table S4, Supporting Information) confirm the same trend: the HEP catalyst exhibits the lowest activation energy of 64 kJ mol^{-1} and the highest TOF of 0.3 s^{-1}.

We also built and compared the catalysts on Au-coated Ni foam and Ni foam. In neutral electrolyte, the HEP catalyst outperforms both IrO_2 and other relevant controls (Figure 2e; Table S1 and Figure S11, Supporting Information). The HEP catalyst on Au-coated Ni foam achieves a 310 mV at current density 10 mA cm^{-2} compared to 344 mV for Ni–Fe and 360 mV for HEL Ni–Fe–Ba. We measured R_s and R_{ct} to identify the effect of supports on catalytic performance. The Au-coated Ni foams have the lowest R_s and R_{ct}, consistent with the view that it provides faster charge transfer (Table S5 and Figure S12, Supporting Information).

We further tested the *iR*-corrected LSV curves on GCE and Au-coated Ni foam to exclude the effects of cell geometry measurement and conductivity on performance (Figure S13, Supporting Information). The HEP Ni–Fe–Mg catalyst requires of 290 mV overpotential at 10 mA cm^{-2} on Au-coated Ni foam after *iR*-correction, which is 35 mV lower than that of Ni–Fe catalyst and 50 mV lower than that of HEL Ni–Fe–Ba catalyst). Ni and Fe K-edge X-ray absorption near-edge structure spectroscopy and Fourier-transformed extended X-ray absorption fine structure spectra of catalysts showed no obvious change for Ni–Fe–Mg versus relevant controls (Figures S8c–f and S14 and Table S6, Supporting Information). This indicates that the effects of dopants on the electronic structure of Ni and Fe sites do not play a principal role in the observed catalytic enhancement.

We characterized the operating stability of the HEP catalyst at 10 mA cm^{-2} and found that it retained its overpotential to within 10 mV following 900 h of continuous water splitting operation (Figure 2f). The Faradaic efficiency for oxygen production remained at 98% ± 2% throughout.

Investigations of the HEP effect. To explore further the relationship between the hydration effect and catalyst activity, we examined the role of Mg and Ba in water adsorption and water dissociation. When we increase pH, the catalytic advantage from HEP Ni–Fe–Mg is reduced, consistent with the abundance of OH^- at high pH (Table S7, Supporting Information; **Figure 3**a,b), and also in accordance with the viewpoint that alkaline earth cations cannot improve the alkaline catalytic performance.[37,38] The Tafel slope decreased from 150 mV dec^{-1} (pH = 7.2) to 120 mV dec^{-1} (pH = 8.5) and 80 mV dec^{-1} (pH = 14, Figure 3c), which again supports the view that the HEP advantage is occurred in neutral electrolyte.[39–41]

We then characterized the activation energy (E_a) for HEP and HEL catalysts in H_2O and D_2O to evaluate the role of OH/OD bond breaking throughout the OER process based. We leveraged the kinetic isotope effect in these studies. We found that reactions in D_2O present a larger activation energy compared to those in H_2O ($E_a(D_2O) = \approx 1.4\ E_a(H_2O)$, Figure 3d). This difference in the E_a indicates that OH (or OD) bond breaking is the rate-limiting step in the neutral OER process.[42]

We next proceeded to characterize the effect of HEP/HEL metal cations on water adsorption. Fourier transform infrared (FTIR) spectroscopy and X-ray photoelectron spectroscopy

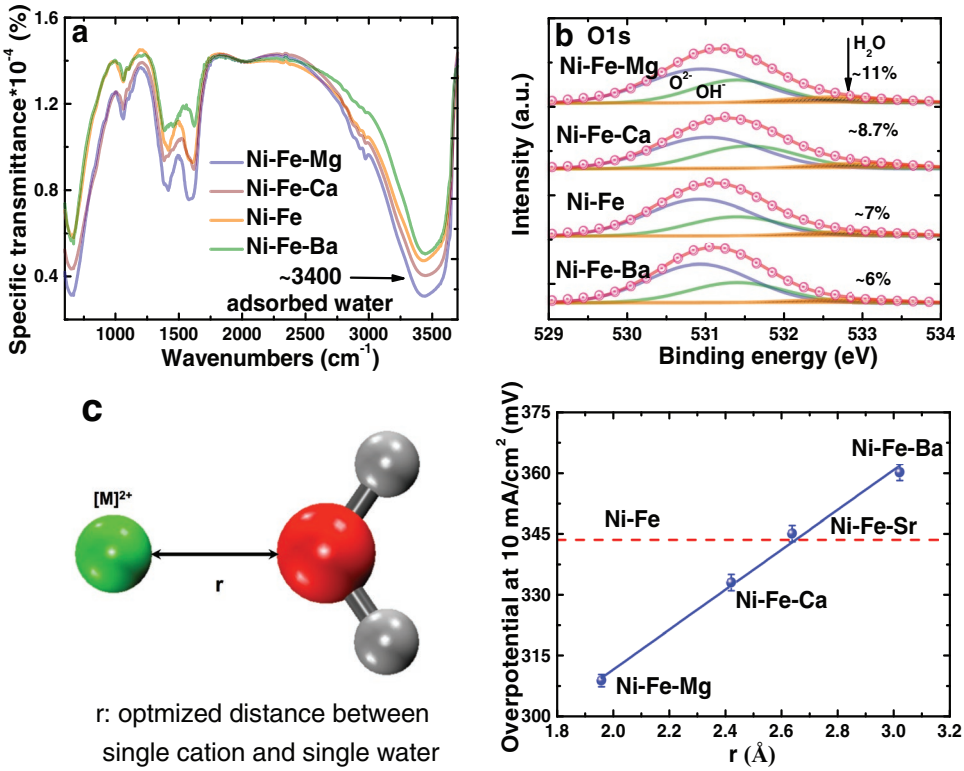

Figure 4. Experimental data regarding the hydration effect. a) FTIR spectra of Ni–Fe–Mg catalyst and relevant controls. b) O1s XPS of Ni–Fe–Mg catalyst and relevant controls. We used the Gaussian fitting to obtain the contribution of the adsorbed water to the XPS spectrum. High magnitude of the H_2O peak in Ni–Fe–Mg spectrum demonstrates higher water adsorption ability of this material. c) This plot reports the distance between single metal ions (Mg, Ca, Sr, and Ba) and one water molecule. The plot reports these distances as a function of the overpotential at 10 mA cm^{-2} current density on Au-coated Ni foam. The correlation was obtained based on a least-square fit. The coefficient of the determinant R^2 was calculated through $R^2 = 1 - SS^{res}/SS^{tot}$, where SS^{res} is the residual sum of squares and SS^{tot} is the total sum of squares.

(XPS) were used to compare the adsorbed water on HEP Ni–Fe–Mg and relevant controls (**Figure 4**a,b). The enhanced peak intensity at ≈3400 cm^{-1} indicates that the HEP Ni–Fe–Mg catalyst favors water molecule adsorption (Figure 4a; Figure S15, Supporting Information).[43] XPS curves indicate large quantities of water adsorbed on the HEP catalyst (Figure 4b).[44,45] Contact angles measurements results show that the addition of Mg^{2+} improves the contact between the electrolyte and the catalyst surface, resulted by the enhanced water-adsorption ability (Figure S16, Supporting Information).

To challenge the role of hydration effect metal cations, we doped other alkaline earth metals into the Ni–Fe framework and characterized OER catalytic activity under identical conditions. The doping concentration of M (Mg, Ca, Sr, and Ba) ratio was fixed at similar value to avoid the effect of dopant concentration on electrochemical activity and water adsorption (Table S8, Supporting Information). The HEP Ni–Fe–Mg and Ni–Fe–Ca catalysts exhibit better performance than HEL Ni–Fe–Sr and Ni–Fe–Ba (Figure 4c). To investigate the hydration-promotion effect further, we performed FTIR and XPS of Ni–Fe–Ca catalyst. The obtained results indicate that the Ni–Fe–Ca catalyst provides improved water-adsorption ability compared to Ni–Fe (Figure 4a,b). Its overpotential of 330 mV at the current density of 10 mA cm^{-2} on Au-coated Ni foam is also lower than that of reference sample (345 mV) (Figure S17, Supporting Information).

In summary, a series of Ni–Fe based catalysts were prepared via a sol–gel method at room temperature, and then used as electrocatalysts for OER in neutral electrolyte. By combining electrochemical characterization with density functional theory (DFT) studies, we found that incorporating hydration effect metal cations into a Ni–Fe framework—namely, the Ni–Fe–Mg catalysts—influences water adsorption and enhances OER performance in neutral electrolytes. Specifically, OER activities on the RHE scale for Ni–Fe based catalysts are increased when we decrease the metal–oxygen distance, consistent with the view that the hydration-effect-promoting water adsorption triggers more favorable OER reaction pathways. In the future, the hydration-effect-promoting phenomenon can be extended to provide enhanced water adsorption for other electrochemical reactions, such as in CO_2 reduction to hydrocarbons, N_2 reduction to ammonia, and other reactions involving water molecules.

Experimental Section

See the details in the Supporting Information.

Supporting Information

Supporting Information is available from the Wiley Online Library or from the author.

Acknowledgements

N.W., Z.C., and X.Z. contributed equally to this work. This work was supported by the Ontario Research Fund – Research Excellence Program, the Natural Sciences and Engineering Research Council of Canada, and the CIFAR Bio-Inspired Solar Energy program. N.W. and X.D.Z. acknowledge support from International Cooperation Projects of the Ministry of Science and Technology (2014DFE60170), National Natural Science Foundation of China (61474065), and (61674084), Tianjin Research Key Program of Science and Technology (18ZXJMTG00220), 111 Project (B16027), and Fundamental Research Funds for the Central Universities. B.Z. and H.S.P. acknowledge funding from Ministry of Science and Technology (2016YFA0203302), the National Natural Science Foundation of China (21875042), and the Program for Professor of Special Appointment (Eastern Scholar) at Shanghai Institutions of Higher Learning and Science and Technology Commission of Shanghai Municipality (18QA1400800). This work benefited from access to the 1W1B beamline at Beijing Synchrotron Radiation Facility. The TEM studies in this work were supported by Jingshan Luo. The simulations were performed using the KAUST supercomputer (HPC).

Conflict of Interest

The authors declare no conflict of interest.

Keywords

hydration effect, neutral electrolytes, Ni–Fe catalysts, oxygen evolution reaction

Received: October 16, 2019
Revised: December 11, 2019
Published online:

[1] B. M. Hunter, H. B. Gray, A. M. Muller, *Chem. Rev.* **2016**, *116*, 14120.
[2] J. Suntivich, K. J. May, H. A. Gasteiger, J. B. Goodenough, Y. Shao-Horn, *Science* **2011**, *334*, 1383.
[3] A. Grimaud, O. Diaz-Morales, B. Han, W. T. Hong, Y.-L. Lee, L. Giordano, K. A. Stoerzinger, M. T. M. Koper, Y. Shao-Horn, *Nat. Chem.* **2017**, *9*, 457.
[4] R. Subbaraman, D. Tripkovic, K. C. Chang, D. Strmcnik, A. P. Paulikas, P. Hirunsit, M. Chan, J. Greeley, V. Stamenkovic, N. M. Markovic, *Nat. Mater.* **2012**, *11*, 550.
[5] C. Liu, B. C. Colón, M. Ziesack, P. A. Silver, D. G. Nocera, *Science* **2016**, *352*, 1210.
[6] M. W. Kanan, D. G. Nocera, *Science* **2008**, *321*, 1072.
[7] K. S. Joya, Y. F. Joya, H. J. M. De Groot, *Adv. Energy Mater.* **2014**, *4*, 1301929.
[8] K. Li, J. Zhang, R. Wu, Y. Yu, B. Zhang, *Adv. Sci.* **2016**, *3*, 1500426.
[9] H. Schäfer, D. M. Chevrier, P. Zhang, J. Stangl, K. Müller-Buschbaum, J. D. Hardege, K. Küpper, J. Wollschläger, U. Krupp, S. Dühnen, *Adv. Funct. Mater.* **2017**, *26*, 6402.
[10] Z. Zhang, J. Hao, W. Yang, J. Tang, *RSC Adv.* **2016**, *6*, 9647.
[11] K. Xu, C. Han, L. Liu, H. Lv, X. Wu, C. Wu, Y. Xie, *Nano Lett.* **2017**, *17*, 578.
[12] M. Bajdich, M. Garcia-Mota, A. Vojvodic, J. K. Norskov, A. T. Bell, *J. Am. Chem. Soc.* **2013**, *135*, 13521.
[13] M. Schreier, L. Curvat, F. Giordano, L. Steier, A. Abate, S. M. Zakeeruddin, J. Luo, M. T. Mayer, M. Grätzel, *Nat. Commun.* **2015**, *6*, 7326.
[14] P. Chen, K. Xu, T. Zhou, Y. Tong, J. Wu, H. Cheng, X. Lu, H. Ding, C. Wu, Y. Xie, *Angew. Chem., Int. Ed.* **2016**, *55*, 2488.
[15] A. M. Smith, L. Trotochaud, M. S. Burke, S. W. Boettcher, *Chem. Commun.* **2015***51*, 5261.
[16] B. Zhang, Y. H. Lui, H. Ni, S. Hu, *Nano Energy* **2017**, *38*, 553.
[17] A. Yamaguchi, R. Inuzuka, T. Takashima, T. Hayashi, K. Hashimoto, R. Nakamura, *Nat. Commun.* **2014**, *5*, 4256.
[18] R. D. L. Smith, M. S. Prevot, R. D. Fagan, Z. Zhang, P. A. Sedach, K. J. S. Man, S. Trudel, C. P. Berlinguette. *Science* **2013**, *340*, 60.
[19] D. T. Limmer, A. P. Willard, P. Madden, D. Chandler, *Proc. Natl. Acad. Sci. USA* **2013**, *110*, 4200.
[20] C. Zhen, R. Kumar, Y. Peng, G. A. Voth, *J. Phys. Chem. C* **2015**, *119*, 14675.
[21] J. Carrasco, A. Hodgson, A. Michaelides, *Nat. Mater.* **2012**, *11*, 667.
[22] D. Strmcnik, K. Kodama, D. Van Der Vliet, J. Greeley, V. R. Stamenkovic, N. M. Markovic, *Nat. Chem.* **2009**, *1*, 466.
[23] C. Stoffelsma, P. Rodriguez, G. Garcia, N. Garciaaraez, D. Strmcnik, N. M. Marković, M. T. M. Koper, *J. Am. Chem. Soc.* **2010**, *132*, 16127.
[24] Z. Shen, Y. Liu, P. E. Brown, I. Szlufarska, H. Xu, *J. Phys. Chem. C* **2014**, *118*, 15716.
[25] Y. Elbaz, M. C. Toroker, *J. Phys. Chem. C* **2017**, *121*, 16819.
[26] J. C. Conesa, *J. Phys. Chem. C* **2016**, *120*, 18999.
[27] V. Fidelsky, M. C. Toroker, *Phys. Chem. Chem. Phys.* **2017**, *19*, 7491.
[28] M. Bajdich, M. García-Mota, A. Vojvodic, J. K. Nørskov, A. T. Bell, *J. Am. Chem. Soc.* **2013**, *135*, 13521.
[29] B. Zhang, X. Zheng, O. Voznyy, R. Comin, M. Bajdich, M. García-Melchor, L. Han, J. Xu, M. Liu, L. Zheng, F. P. García de Arquer, C. T. Dinh, F. Fan, M. Yuan, E. Yassitepe, N. Chen, T. Regier, P. Liu, Y. Li, P. De Luna, A. Janmohamed, H. L. Xin, H. Yang, A. Vojvodic, E. H. Sargent, *Science* **2016**, *352*, 333.
[30] X. Ji, L. Cui, D. Liu, S. Hao, J. Liu, F. Qu, Y. Ma, G. Du, A. M. Asiri, X. Sun, *Chem. Commun.* **2017**, *21*, 3070.
[31] X. Zheng, B. Zhang, P. D. Luna, Y. Liang, R. Comin, O. Voznyy, L. Han, F. P. G. d. Arquer, M. Liu, C. T. Dinh, T. Regier, J. Dynes, S. He, H. L. Xin, H. S. Peng, D. Prendergast, X. W. Du, E. H. Sargent, *Nat. Chem.* **2018**, *10*, 149.
[32] H. Li, S. Chen, X. Jia, B. Xu, H. Lin, H. Yang, L. Song, X. Wang, *Nat. Commun.* **2017**, *8*, 15377.
[33] C. C. McCrory, S. Jung, J. C. Peters, T. F. Jaramillo, *J. Am. Chem. Soc.* **2013**, *135*, 16977.
[34] M. S. Burke, L. J. Enman, A. S. Batchellor, S. Zou, S. W. Boettcher, *Chem. Mater.* **2016**, *47*, 7549.
[35] M. B. Stevens, L. J. Enman, A. S. Batchellor, M. R. Cosby, A. E. Vise, C. D. M. Trang, S. W. Boettcher, *Chem. Mater.* **2017**, *29*, 120.
[36] A. S. Batchellor, S. W. Boettcher, *ACS Catal.* **2015**, *5*, 6680.
[37] L. J. Enman, M. S. Burke, A. S. Batchellor, S. W. Boettcher, *ACS Catal.* **2016**, *6*, 2416.
[38] J. Zaffran, M. B. Stevens, C. D. M. Trang, M. Nagli, M. Shehadéh, S. W. Boettcher, M. C. Toroker, *Chem. Mater.* **2017**, *29*, 4761.
[39] J. M. Hu, J. Q. Zhang, C. N. Cao, *Int. J. Hydrogen Energy* **2004**, *29*, 791.
[40] L. M. D. Silva, J. F. C. Boodts, L. A. D. Faria, *Electrochim. Acta* **2001**, *46*, 1369.
[41] I. M. Sadiek, A. M. Mohammad, M. E. El-Shakre, M. S. El-Deab, *Int. J. Hydrogen Energy* **2012**, *37*, 68.
[42] L. Melander, W. H. Saunders, Wiley, New York **1980**, 126.
[43] H. A. Al-Hosney, V. H. Grassian, *Phys. Chem. Chem. Phys.* **2005**, *7*, 1266.
[44] G. Gaggiotti, A. Galdikas, S. Kačiulis, G. Mattogno, A. Šetkus, *J. Appl. Phys.* **1994**, *76*, 4467.
[45] Y. Nagasawa, T. Choso, T. Karasuda, *Surf. Sci.* **1999**, *433*, 226.